Paleoceanography and Paleoclimatology

AGU ADVANCING EARTH AND SPACE SCIENCE

RESEARCH ARTICLE
10.1029/2021PA004385

Key Points:

- Iron fertilization of GoA waters linked to Cordilleran Ice Sheet iceberg discharge as driver of phytoplankton growth during the past 54 ka
- Occurrence of calcareous and siliceous primary producers was largely unaffected by low SST conditions during MIS 3 and MIS 2
- The impact of tidewater glaciers on marine productivity of high-latitude coastal regions is essential to understand land-ocean interactions

Supporting Information:

Supporting Information may be found in the online version of this article.

Correspondence to:

O. E. Romero,
oromero@marum.de

Citation:

Romero, O. E., LeVay, L. J., McClymont, E. L., Müller, J., & Cowan, E. A. (2022). Orbital and suborbital-scale variations of productivity and sea surface conditions in the Gulf of Alaska during the past 54,000 years: Impact of iron fertilization by icebergs and meltwater. *Paleoceanography and Paleoclimatology*, *37*, e2021PA004385. https://doi.org/10.1029/2021PA004385

Received 8 JUL 2021
Accepted 21 DEC 2021

Author Contributions:

Conceptualization: Oscar E. Romero, Leah J. LeVay, Erin L. McClymont, Juliane Müller, Ellen A. Cowan
Formal analysis: Oscar E. Romero, Leah J. LeVay, Erin L. McClymont, Juliane Müller, Ellen A. Cowan
Funding acquisition: Oscar E. Romero, Leah J. LeVay, Erin L. McClymont, Juliane Müller, Ellen A. Cowan

Orbital and Suborbital-Scale Variations of Productivity and Sea Surface Conditions in the Gulf of Alaska During the Past 54,000 Years: Impact of Iron Fertilization by Icebergs and Meltwater

Oscar E. Romero[1,2], Leah J. LeVay[3], Erin L. McClymont[4], Juliane Müller[1,2], and Ellen A. Cowan[5]

[1]MARUM – Center for Marine Environmental Sciences, University of Bremen, Bremen, Germany, [2]Alfred Wegener Institute, Helmholtz Centre for Polar and Marine Research, Bremerhaven, Germany, [3]International Ocean Discovery Program, Texas A&M University, College Station, TX, USA, [4]Department of Geography, Durham University, Durham, UK, [5]Department of Geological and Environmental Sciences, Appalachian State University, Boone, NC, USA

Abstract As a high-nutrient and low-chlorophyll region, the modern Gulf of Alaska (GoA) is strongly impacted by the limitation of iron. Paleostudies along the Alaskan slope have mainly focused on reconstructing environmental conditions over the past 18 ka. Based on micropaleontological, biogeochemical, and sedimentological parameters, we explore a sediment record covering the past 54 ka at Integrated Ocean Drilling Program Site U1419 to understand the impact of orbital- and suborbital-scale climate variability on productivity and sea-surface conditions. Close to the Cordilleran Ice Sheet (CIS), Site U1419 is ideally located to elucidate how the evolution of a large ice mass and glacial processes affected orbital- and suborbital-scale changes in nutrients (e.g., iron) supply. Meltwater discharge from the northern CIS impacted sea surface dynamics of GoA coastal waters. The corresponding increases in bulk biogenic concentrations during Marine Isotope Stage (MIS) 3 and MIS 2 (54–17 ka) suggests a direct impact from iron fertilization. The lack of a consistent relationship between productivity and SST suggests that cooling of surface waters was not the dominant control on primary producers. The inundation of the subaerially exposed continental shelf during the last deglacial (17–10 ka) warming could have served as a major micronutrient source, accounting for a deglacial peak in production. Low productivity after the last deglaciation suggests reduced iron availability, which we link to reduced meltwater inputs from smaller ice masses onshore. Our multiproxy approach reveals a more comprehensive picture of late Quaternary productivity variations compared to earlier studies along the Alaskan margin. The impact of tidewater glaciers and meltwater discharge on past marine productivity and nutrient budget dynamics of high-latitude coastal regions is discussed.

1. Introduction

Located in the subarctic eastern Pacific, the Gulf of Alaska (GoA) is a high-nutrient, low-chlorophyll (HNLC) area where phytoplankton biomass is consistently low (Childers et al., 2005). Especially beyond the continental shelf break, coastal surface waters of the GoA are largely iron-limited (Boyd et al., 2007). As low bioavailability of the micronutrient iron critically limits the occurrence of primary producers (Martin, 1990), present-day increases in the iron supply mostly led to enhanced productivity in surface waters and carbon export to the seafloor of the GoA (Childers et al., 2005; Coyle et al., 2019; Strom et al., 2006, 2016). Iron fertilization is widely acknowledged to enhance primary productivity in high northern (Strom et al., 2006, 2016) and southern (Blain et al., 2007; Duprat et al., 2016) latitudes. Glaciers play a globally significant role as a source of iron to the marine surface waters (Hopwood et al., 2015). While marine sediment records show higher paleoproduction during glacials that are correlated with enhanced iron inputs in high southern latitudes (e.g., Martínez-García et al., 2011), paleoceanographic records supporting links between productivity and glacier dust and/or iceberg discharge-mediated iron fertilization in the north-eastern Pacific Ocean are still scarce (Müller et al., 2018).

Paleoclimate reconstructions based on sediments deposited beneath waters close to the Alaskan margin have mainly focused on the physical and biological changes throughout the last deglaciation and the Holocene (Addison et al., 2012; Barron et al., 2009; Davies et al., 2011; Praetorius et al., 2018). However, it is still unclear how marine productivity and sea-surface conditions of GoA coastal waters responded to pulses of meltwater and

Investigation: Oscar E. Romero, Leah J. LeVay, Erin L. McClymont, Juliane Müller, Ellen A. Cowan
Methodology: Oscar E. Romero, Leah J. LeVay, Erin L. McClymont, Juliane Müller, Ellen A. Cowan
Resources: Oscar E. Romero, Leah J. LeVay, Erin L. McClymont, Juliane Müller, Ellen A. Cowan
Supervision: Oscar E. Romero, Leah J. LeVay, Erin L. McClymont, Juliane Müller, Ellen A. Cowan
Validation: Oscar E. Romero, Leah J. LeVay, Erin L. McClymont, Juliane Müller, Ellen A. Cowan
Visualization: Oscar E. Romero, Leah J. LeVay, Erin L. McClymont, Juliane Müller, Ellen A. Cowan
Writing – original draft: Oscar E. Romero, Leah J. LeVay, Erin L. McClymont, Juliane Müller, Ellen A. Cowan
Writing – review & editing: Oscar E. Romero, Leah J. LeVay, Erin L. McClymont, Juliane Müller, Ellen A. Cowan

iceberg discharge during Marine Isotope Stages (MIS) 2 and 3, when the Cordilleran Ice Sheet (CIS) was larger than present (Seguinot et al., 2016). Since primary producers which occur in surface waters of the GoA north of 57°N are largely influenced by iron limitation (Boyd et al., 2007; Martin, 1990; Strom et al., 2006, 2016), understanding the delivery and impact of micronutrients in past geological times can be helpful in interpreting future trends of phytoplankton growth in response to global change. A remarkable recent discovery is that millennial-scale episodes of reorganized Pacific Ocean ventilation at Site U1419 occurred in phase with large deliveries of CIS ice-rafted debris (IRD) during the past 42 ka, indicating a close linkage between ice and ocean dynamics (Walczak et al., 2020). These intervals of increased IRD accumulation, termed Siku Events (SE), precede North Atlantic Heinrich Events (HE) by ∼1,300 years (Walczak et al., 2020). Since meltwater delivers iron to the GoA (Childers et al., 2005; Crusius et al., 2011, 2017), these episodic iceberg discharges along the northern Alaskan margin might have also impacted the past nutrient availability of surface waters overlying Site U1419.

Relative to many other areas of the subarctic Pacific Ocean, the northern GoA remains under-studied (Crusius et al., 2017). This limits our understanding of the important processes controlling (paleo)productivity variations in the high-latitude Pacific such as the impact of iceberg discharge and the potential importance of bioavailable iron delivery to this HNLC area. This study presents a high-resolution paleorecord of primary productivity and sea-surface temperatures (SST) for the past 54 ka at Integrated Ocean Drilling Program (IODP) Site U1419 (ca. 59°N, 145°W, Figure 1). We combine independent biogenic parameters indicative of variations of (a) ocean productivity (coccolithophorids, diatoms, bulk biogenic components), (b) sea-ice cover (IP_{25}, $C_{37:4}$, diatoms), and (c) alkenone-based ($U^{K'}_{37}$ -) SST, and compare these to the Site U1419 IRD record (Walczak et al., 2020). Our findings describe glacial-interglacial and millennial-scale changes in productivity as well as potential sources of nutrient inputs, offering new evidence which help interpret the drivers of environmental change in the GoA during the last 54 ka.

2. Study Area

2.1. Atmospheric and Hydrographic Settings, and Ice Dynamics

Surface waters overlying Site U1419 are iron-poor, nitrate-rich, and have low chlorophyll concentrations. Two nutrient regimes are known in the GoA: a HNLC region in the center of the Alaska Gyre, offshore of the Alaskan coast; and a low nutrient, high chlorophyll regime which is associated with the Alaska Coastal Current (ACC) (Childers et al., 2005). These regimes are characterized by specific oceanographic conditions. Advection of deep eutrophic waters to the surface ocean coupled with micronutrient availability (i.e., iron) from land is typical of the HNLC region, while the low-nutrient, high chlorophyll region relies on the advection of deep, nutrient-rich waters to supply macronutrients (i.e., nitrate) (Childers et al., 2005; Stabeno et al., 2004).

An annual cycle of nutrient drawdown and replenishment occurs in the euphotic zone of waters overlying Site U1419, in response to the local ocean circulation. Wind-induced downwelling and easterly coastal winds cause a well-mixed water column in winter (Childers et al., 2005). Phytoplankton blooms are associated with the onset of annual stratification in spring/summer, when increased light availability favors high productivity (Henson, 2007). An autumnal peak in chlorophyll concentrations is observed with the initial weakening of stratification (Henson, 2007). Although freshwater input associated with glacier meltwaters causes stratification of the upper water column (Stabeno et al., 2004), it also fertilizes the ocean surface (Crusius et al., 2017). Presently, mostly land-derived rainfall water is transported along the southwest Alaskan coast through the ACC (Kipphut, 1990).

The circulation in the GoA is dominated by a two-current system: the subarctic gyre in the ocean basin, including the Alaska Current (AC), and the ACC on the continental shelf (Figure 1; Stabeno et al., 2004). The ACC flows northwards along the Alaskan continental shelf, forced by alongshore winds, and it is fueled with large freshwater runoff by glacier and river discharge (Crusius et al., 2017; Stabeno et al., 2004). The AC is sourced from warm mid-latitude currents of the North Pacific flowing eastwards, termed the North Pacific Current (Stabeno et al., 2004). The AC turns south-westward at the northern border of the GoA and forms the beginning of the Alaskan Stream (Freeland, 2006; Stabeno et al., 2004). The flow of water masses in the study area is further complicated by small, transient eddies frequenting the GoA shelf, which combine with large, long-lasting eddies that travel along the continental slope for 2–3 years (Crawford et al., 2007). These eddies may also influence transport and mixing of nutrients to the euphotic zone of the GoA.

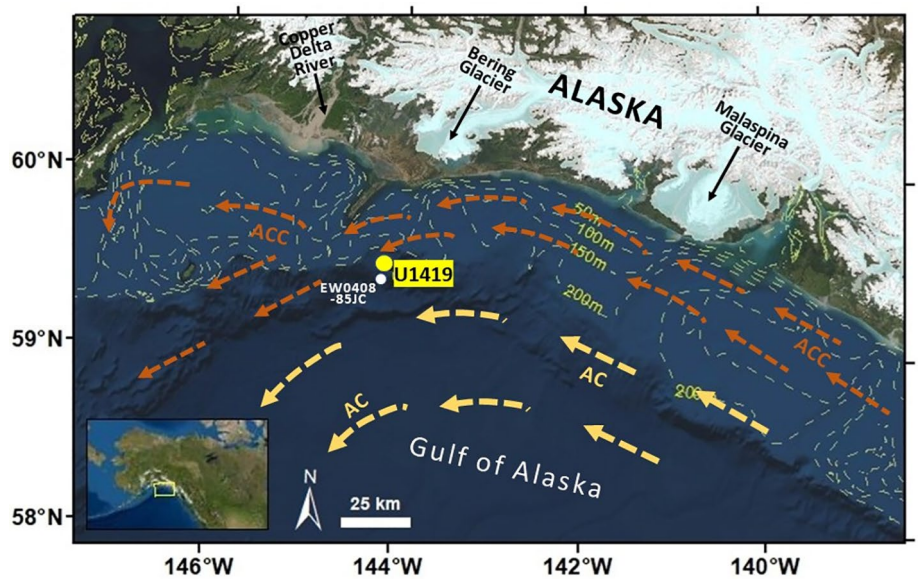

Figure 1. Map showing the study area in the high latitude north-eastern Pacific Ocean. Location of IODP Site U1419 (yellow dot, 59°31.9′N, 144°8.0′W; 698 m depth; Expedition 341, Jaeger, Gulick, & LeVay, 2014) and EW0408-85JC (white dot; Addison et al., 2012; Barron et al., 2009; Davies et al., 2011; Praetorius et al., 2018). AC: Alaska Current; ACC: Alaska Coastal Current.

Iron sources to the euphotic zone in the GoA are: atmospheric dust, glacier flour (fine ground dust containing Fe) derived from meltwater and iceberg rafting (Müller et al., 2018), shallow shelf sediments (Crusius et al., 2011), hydrothermal inputs (Boyd & Ellwood, 2010) and eddies (Crusius et al., 2017). An immediate response of phytoplankton to iron fertilization (Boyd et al., 2007) is indicated by a twofold increase in the particulate organic matter C:N ratio when iron is available (Martin, 1990). In coastal GoA waters, delivery of bioavailable iron has four main sources: (a) glacier flour transported by rivers (Crusius et al., 2011), (b) dust from exposed glacial sediments and river mouths during the fall (such as the Copper River, Crusius et al., 2011), (c) sea level rise and associated flooding (Davies et al., 2011), and (d) sediments stored on the shelf and slope (Praetorius et al., 2015). Glacial meltwater dominates delivery of dissolved iron to the coastal GoA (Schroth et al., 2009). For the purpose of this paper and according to Crusius et al. (2017), the terms "meltwater," "glacial meltwater," and "freshwater" are considered synonymous and primarily reflect discharge from rivers which has originated from glacier melt.

Freshwater discharge into the coastal GoA strongly varies on seasonal and interannual timescales (Wang et al., 2004). From November to April, winter precipitation is mainly stored as snow, and freshwater discharge is reduced to a minimum. Freshwater discharge rises sharply from May due to (a) increasing precipitation and (b) above-freezing temperatures. Summer discharge remains high until September because of melting snow and some glacier melt. River discharge decreases rapidly in October, and reaches a basic flow in December as temperatures drop below 0°C (Wang et al., 2004).

3. Materials and Methods

3.1. Site U1419

In May–July 2013, IODP Expedition 341 drilled a transect of sites (U1417-U1421) in the GoA, across the Surveyor Fan to the continental shelf offshore of the St. Elias Mountains. The main objective of Expedition 341 was to investigate a glacially eroded sedimentary record during a cooling climate (Miocene through to Pleistocene) with increasing intensity of glaciations (Jaeger, Gulick, & LeVay, 2014). Site U1419 is located at 59°31.93′N–144°8.03′W and was drilled to 193.72 m CCSF-B (meters core composite depth below sea floor, method B; Jaeger, Gulick, LeVay, et al., 2014) at 698 m water depth on the northern Alaskan continental slope. Here, we focus on the uppermost 47 m (2–54 ka) of the cored sequence, where high recovery (>87%, Jaeger,

Gulick, & LeVay, 2014) allows development of a high-resolution reconstruction of primary production and sea-surface conditions constrained by foraminiferal radiocarbon dates (Walczak et al., 2020).

3.2. Age Model and Sedimentation Rates

The detailed chronology for Site U1419 between the present and ~54 ka is based on 250 radiocarbon dates on pairs of benthic-planktic foraminifera spanning the past ~50 ka and 28 paired measurements from <18 ka in the co-located core EW0408-85JC (Walczak et al., 2020). The incorporation of radiocarbon data from EW0408-85JC onto the U1419 depth scale increases the resolution of dates available for the age model in the Holocene and the Last Glacial Maximum. While the age model remains well constrained before 42 ka, the analytical uncertainty of both benthic and planktic foraminiferal dates preclude meaningful interpretation of benthic-planktic age differences (Walczak et al., 2020). The Bayesian age model for U1419 sediments was generated using BChron software, which evaluated all available foraminiferal dates and calibrated using the Marine13 calibration curve back to c. 47 ka (Reimer et al., 2013). Radiocarbon measurements on benthic and planktic foraminifera back to 47 ka were calibrated using the IntCal13 curve (Reimer et al., 2013). A constant benthic reservoir correction (R) of 1200 ± 600 years was used (Walczak et al., 2020), whereas a variable planktic reservoir correction (R) (average 370 ± 350 years) reflected modeled circulation changes and the measured benthic—planktic differences in the core. The age model has an average 1σ-uncertainty of 210 cal. year. For the interval 47–54 ka, Walczak et al. (2020) introduced an ad-hoc correction to their calendar ages by adding 1200 years to the original calibrated date. Ages for the interval 47–54 ka therefore have additional inaccuracies, particularly when interpreting data at the suborbital scale, and limits the interpretation of our results whenever suborbital scale events occurred in this interval.

The Mass Accumulation Rates (MARs) calculated in this study (Figures 2 and Supporting Information S1) use the 50th percentile values of Walczak et al. (2020). This avoids interpretive artifacts associated with varying sample resolution. All data presented here refer to the calibrated ages.

3.3. Bulk Sediment Components

Biogenic silica (bSi, opal) was measured using a sequential leaching technique in the Marum Opallab (University of Bremen, Bremen, Germany) (Müller & Schneider, 1993). The precision of the sequential leaching technique is better than 0.5% (Müller & Schneider, 1993). The resolution of bSi measurements (at least every 40 cm) is lower than the diatom counts (every 10–40 cm). This is because the diatom values are at/close to zero in many Site U1419 samples, thus making the bSi content almost undetectable (Müller & Schneider, 1993). The precision of the overall method based on replicate analyses is mostly between ±0.2% and ± 0.4%, depending on the composition of the material analyzed. For standard deviations of bSi measurements we refer to Müller and Schneider (1993).

The total organic carbon content (wt. % TOC) was determined by means of a Vario MAX C elemental analyzer after decalcification with 1.3 N hydrochloric acid. Inorganic carbon (% carbonate) was measured using coulometry at the Department of Geological Sciences, University of Florida (Gainesville, Florida, USA) and at the International Ocean Discovery Program, Texas AandM University (College Station, Texas, USA). In total, 284 samples were dried in an oven at 50°C, ground with a mortar and pestle, weighed on a microbalance, and digested using 2 N HCl. The coulometer measures the micrograms C released from the digestion of the sample. Carbonate is then calculated as $CaCO_3$ = µg C * 8.333/sample mass (µg). Replicate measurements indicate an error of up to 0.19% carbonate.

3.4. Alkenone and IP_{25} Analysis and SST Estimations

Alkenones were extracted from 1 to 2 g freeze-dried and homogenized sediments which had been sampled every 50 cm on average (but as low as every 2 cm), following Kim et al. (2002). Alkenones were analyzed by capillary gas chromatography: a gas chromatograph (HP 5890A) was equipped with a 60 m column (JandW DB1, 0.32 mm × 0.25 µm), a split injector (1:10 split modus), and a flame ionization detector (GC-FID). Quantification of the individual C_{37} alkenone concentrations ($C_{37:2}$, $C_{37:2}$, and $C_{37:4}$) was achieved using nonadecanone as an

internal standard. Although $C_{37:4}$ has been used as an indicator of freshwater inputs to marine environments (e.g., Sánchez-Montes et al., 2020), recently it has been suggested that there is a potential sea-ice contribution to $C_{37:4}$ (Wang et al., 2021). To account for this potentially different source to the alkenone concentrations, we present concentrations of $C_{37:3} + C_{37:2}$ separate from $C_{37:4,}$ although the overall patterns remain the same. The relative abundance of $C_{37:4}$ is expressed as a percentage of the total C37 alkenones (%$C_{37:4}$) (Rosell-Melé et al., 2002).

To determine SSTs using the alkenone unsaturation index $U^{K\prime}_{37}$, alkenones were analyzed by gas chromatography with chemical ionization mass spectrometry (GC-CIMS), following the instrument method described in detail by Sánchez-Montes et al. (2020). The $U^{K}_{37}{}'$ index is calculated from the relative abundances of the di- and tri-unsaturated C_{37} methyl alkenones as defined by Prahl and Wakeham (1987):

$$U^{K\prime}_{37} = \frac{(C_{37:2})}{(C_{37:2} + C_{37:3})}$$

The $U^{K\prime}_{37}$ values were converted into SSTs by applying the core-top compilation of Müller et al. (1998; $U^{K}_{37}{}' = 0.033*T + 0.044$), which aligns closely with a culture calibration (Prahl et al., 1988; $U^{K\prime}_{37} = 0.034*T + 0.039$). Although alternative high-latitude SST calibrations are also available (Supporting Information S1) the same trends are recorded regardless of calibration. Using multiple extractions and analyses of a sediment sample used as a laboratory internal reference from the South Atlantic, the precision of the measurements ($\pm 1\sigma$) was calculated to be better than 0.003 $U^{K\prime}_{37}$ units (or 0.1°C) (Sánchez-Montes et al., 2020).

To also obtain information on past sea-ice conditions at Site U1419, additional samples were studied for the sea-ice diatom-derived monounsaturated highly branched isoprenoid IP_{25} (Belt et al., 2007). After adding 7-hexylnonadecane as internal standard, up to 6 g of sediment were extracted using an Accelerated Solvent Extractor (DIONEX, ASE 200; 100°C, 5 min, 1000 psi) with dichloromethane:methanol (2:1 v/v), and purified via open-column silica chromatography (*n*-hexane). Identification and quantification of IP_{25} was achieved via coupled gas chromatography-mass spectrometry analyses following Müller et al. (2012).

3.5. Diatom Analyses

After freeze-drying of sediments, samples were prepared following the acid-based method by Schrader and Gersonde (1978). Counts of identified species were carried out on permanent slides (Mountex® mounting medium). Several traverses across each slide were systematically tracked to obtain a representative count of valves (between 300 and 450 valves per slide). For the analysis of 251 samples, we use a Zeiss®Axioscop with interference illumination (Marum, University of Bremen). The counting of two replicate slides at ×1000 magnification indicates an analytical error of ≤10.0%. The census procedure and the definition of counting units followed standard methods (Schrader & Gersonde, 1978).

The resulting counts yielded relative abundance (%) of individual diatom taxa (determined as the fraction of the diatom species vs. the total diatom concentration in a particular sample) as well as concentration of valves per g^{-2} (total diatom concentration), calculated as follows:

$$\text{total diatom concentration} = [N] \times [A/a] \times [1/W] \times [V/v]$$

where, [N] number of valves in an known area [a], as a fraction of the total area of a petri dish [A], the sample weight [W] in g, and the final sample volume (V) and sample volume used for the permanent slide (v) (Sancetta & Calvert, 1988).

3.6. Coccolithophore Abundance

Coccolithophore qualitative abundances range from barren to common (Jaeger, Gulick, & LeVay, 2014). Because of the wide range of abundances observed, we used a semi-quantitative methodology to capture the relative concentrations of coccolithophores in each sample. Strewn smear slides were made for 184 samples at ~40 cm resolution. Glass cover slips were adhered to the microscope slides using Norland Optical Adhesive No. 61. Total number of coccoliths per field of view (FOV) were recorded for 50 FOV per slide using a Zeiss®Axioscop A.1

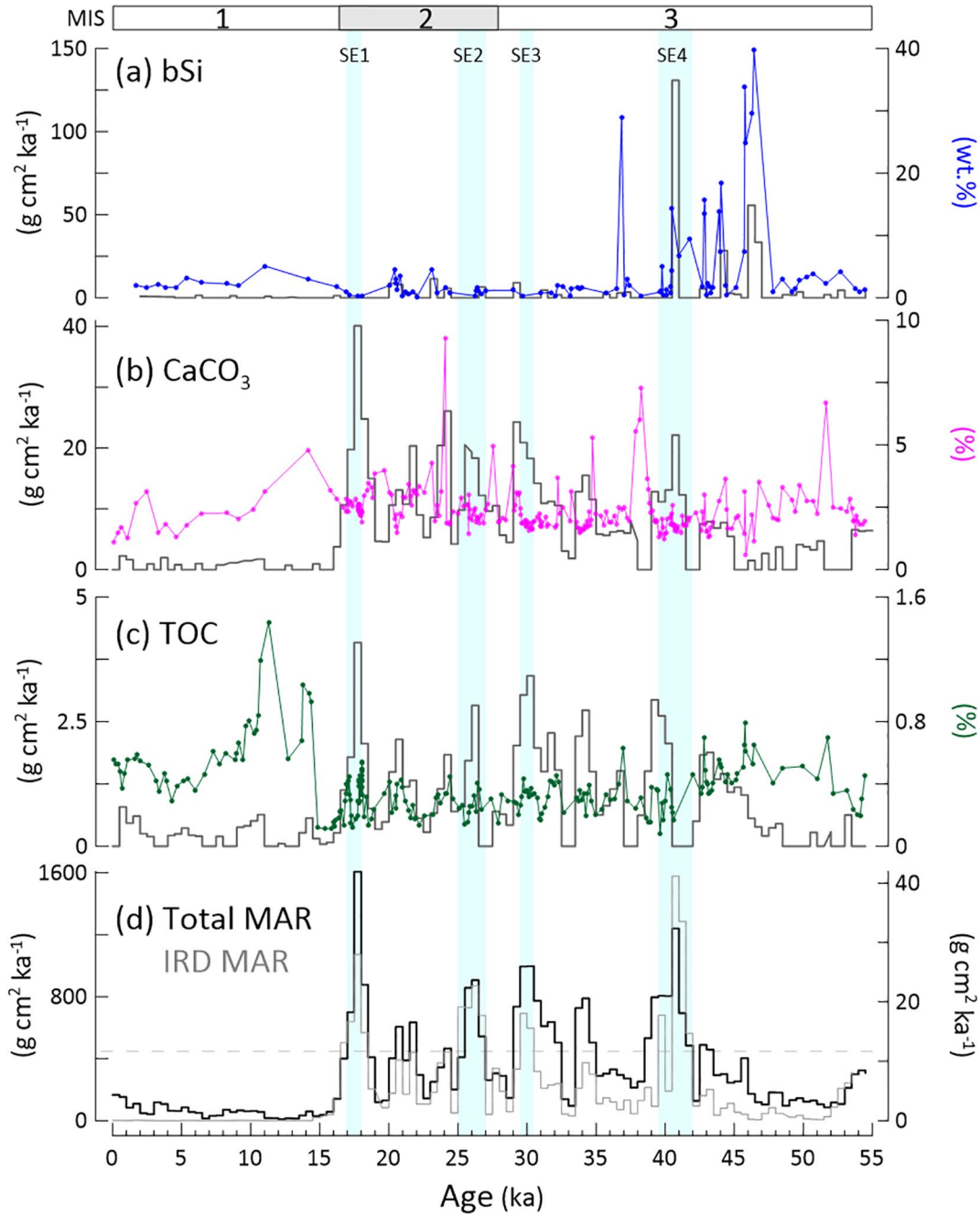

Figure 2. Concentration (lines) and mass accumulation rate (bars) and of bulk biogenic components at IODP Site U1419 for the past 54 ka. (a) bSi (wt.%, blue line, and MAR, g/cm^2/ka, bars); (b) $CaCO_3$ (%, magenta line, and MAR, g/cm^2/ka, bars); (c) total organic carbon (TOC; %, green line, and MAR, g cm^2 ka^{-1}, bars), and (d) total MAR (black line) and ice-rafted debris (IRD) MAR (gray line) (g cm^2 ka^{-1}) from Walczak et al. (2020). After Walczak et al. (2020), MAR is evaluated over constant timestep bins of 500 years to avoid interpretive artifacts associated with varying sample resolution. Light blue bars denote Siku Events (SE) 1–4 where IRD MAR exceeds 12 g cm^2 ka^{-1} (dashed line; Walczak et al., 2020). MIS: Marine Isotope Stages.

at 1,000× magnification. Abundance was recorded as the average number of coccoliths per FOV. While this method does not provide an accurate quantification of flux, it does reflect the relative shifts in high versus low coccolithophore content like qualitative scales (e.g., Bottini & Erba, 2018; Guballa & Peleo-Alampay, 2020). The trends in coccolith FOV abundances follow the % carbonate curve, providing evidence that this method reflects the relative accumulation of coccoliths in sediments.

4. Results

4.1. Bulk Sediment Components

On average, bSi dominated the biogenic fraction of sediments at Site U1419 for the past 54 ka (Figure 2c). The contribution of bSi ranged between 0.1 and 39.8wt.% (average = 4.2 ± 7.3). The contribution of $CaCO_3$ was 0.6%–9.3% (average = 2.3 ±0 .9), and of TOC was 0.1%–1.4% (average = 0.4 ± 0.2).

Except for a few short intervals, values of bSi remained mostly below 5 wt.% (Figure 2b). The highest concentrations (14.0–39.0wt.%) were reached between 46.4 and 36.7 ka. The $CaCO_3$ concentration was higher between late MIS 3 and early MIS 1. Highest maxima of $CaCO_3$ (>5%) occurred at 24.08 ka (9.3%), 34.73 ka (5.3%), 37.85–38.27 ka (5.6–7.3), and 51.66 ka (6.9%). TOC values remained below 0.9% prior to 14.5 ka, increased abruptly at 14.3 ka and reached a maximum of 1.4% at 11.30 ka. From 9.80 ka to the present, TOC values decreased to less than 0.8% (Figure 2b). The concentrations of TOC and bSi showed subtle increases associated with SE 1–4.

Mass Accumulation Rate (MAR) of the measured bulk sedimentary components closely follow the overall pattern of total and ice-rafted debris (IRD) MAR (Figure 2). bSi MAR ranged 0.1–130.9 g cm^{-2} ka^{-1} (average = 14.3 ± 23.8); $CaCO_3$ MAR ranged 0.3–40.9 g cm^{-2} ka^{-1} (average = 8.9 ± 9.1), and the TOC MAR range is 0.01–4.1 g cm^{-2} ka^{-1} (average = 1.2 ± 1.3). Peaks of $CaCO_3$ and TOC MAR better matched the temporal pattern of total MAR than bSi MAR. Carbonate and TOC MARs peaked during SEs (SE) 1–4. The highest MAR for carbonate occurred during SE1 (40.9 g cm^{-2} ka^{-1}) (Figure 2b). TOC MAR peaked during SE1 (4.0 g cm^{-2} ka^{-1}) and SE3 (3.4 g cm^{-2} ka^{-1}) (Figure 2c). Exceptions to this pattern is a $CaCO_3$ MAR peak at c. 24.5 ka (Heinrich stadial 2, 26.1 g/cm^2/ka). Additionally, peaks in both carbon species MAR are observed from 21 to 22 ka and ~34 ka. MAR TOC had an additional maximum between ~42.5 and 43.5 ka (1.8 g cm^{-2} ka^{-1}). The highest bSi MAR (130.1 g cm^{-2} ka^{-1}) occurred at c. 41 ka (SE4, Figure 2c). Two earlier moderate bSi MAR peaks are at c. 46 and 44 ka. The increase in bulk biogenic MAR during the SEs may reflect enhanced preservation due to increased burial rates or the addition of terrestrially derived components. The different temporal patterns between MAR and concentration of bulk sediment components (Figure 2) suggest that these biogenic maxima were impacted by enhanced burial efficiency (promoting organic matter and silica preservation; Hartnett et al., 1998; Ragueneau et al., 2000) caused by high sediment accumulation and/or the meltwater-related discharges from the CIS along the northern Alaska margin (Cowan et al., 2020).

4.2. Coccolithophorid Components and Alkenone Concentration

Coccolith relative abundance ranged from barren (0 coccoliths/FOV) to 332 coccoliths/FOV with an average of 67.53 coccoliths/FOV. The highest abundances occurred at. 51.66 ka (366 coccoliths/FOV), at 42.87 ka (305 coccoliths/FOV) and ~14.5 ka (332 coccoliths/FOV) (Figure 3a). Maxima in coccolith abundances roughly corresponded to SEs (except SE3) and high % carbonate intervals, however, there were exceptions to this trend.

The coccolithophore assemblage was dominated by *Coccolithus pelagicus* and *Geophyrocapsa muellerae*, both of which were found in high latitudes during the Quaternary (McIntyre & Be, 1967; Winter et al., 1994; Ziveri et al., 2004).

The $C_{37:2} + C_{37:3}$ alkenone concentrations ranged from 0.01 to 2.88 μg g^{-1} (Figure 3d). Maximum concentrations were recorded c. 47.5 ka (2.88 μg g^{-1}) and at 10.1–10.6 ka (1.94–1.34 μg g^{-1}), the latter peak marking a period of elevated alkenone concentrations during the deglaciation (c. 9–11 ka). Overall, the lowest concentrations were recorded between 45.5 and 15 ka (<0.27 μg g^{-1}). There was no clear relationship between alkenone concentration and SEs.

4.3. Diatoms

4.3.1. Concentration

The total diatom concentration varied strongly throughout the past 54 ka (range 0–8.3*10^6 valves gr^{-1}, average = 2.5*10^5 valves gr^{-1}±9.8*10^5). The occurrence of diatoms was limited to a few intervals (Figure 3b). The highest concentration range (5.5–8.3*10^6 valves g^{-1}) was reached between 45.78 and 46.43 ka. A second highest maximum (5.7 * 10^6 valves g^{-1}) occurred around 36.84 ka.

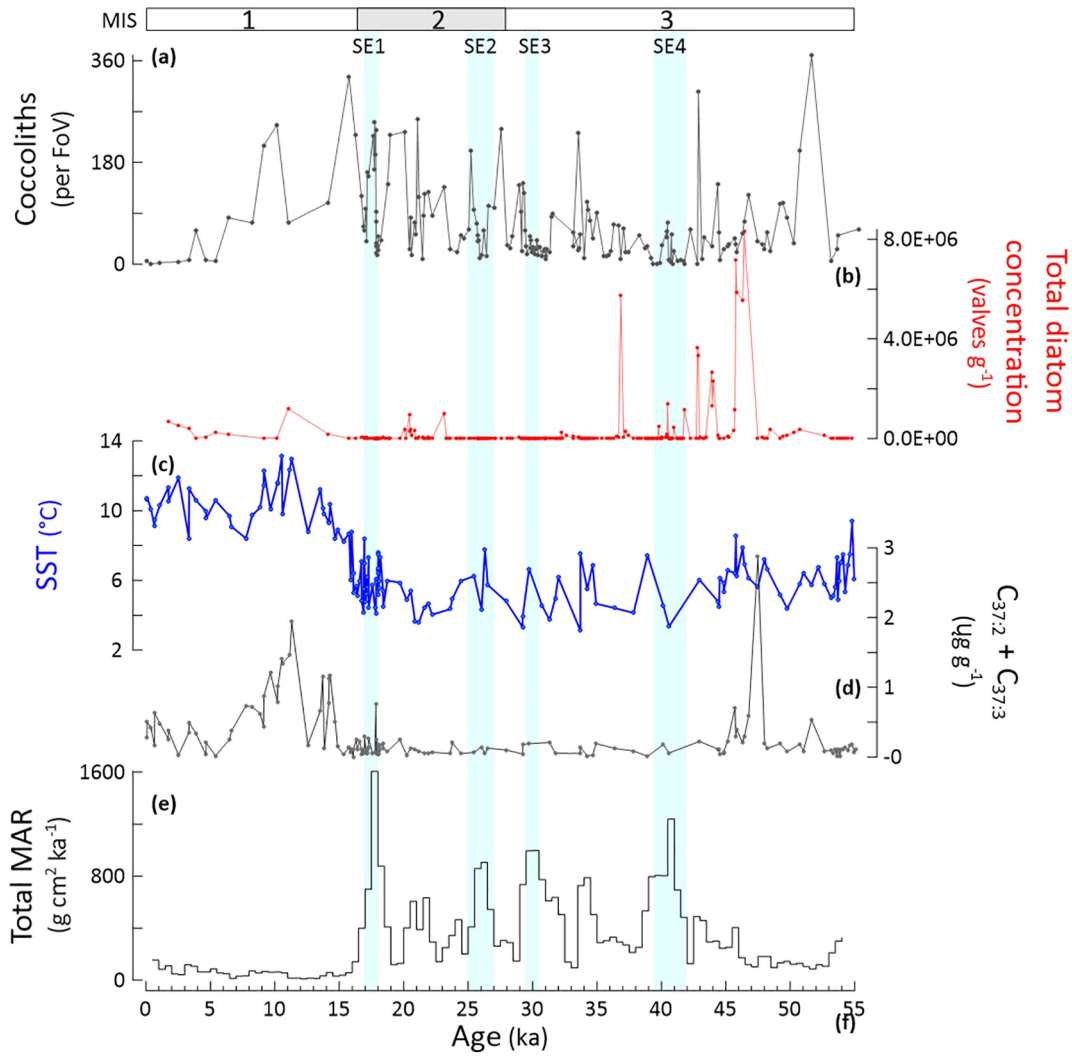

Figure 3. The productivity signal—Concentration of coccoliths and diatoms, reconstructed sea-surface temperature, and $C_{37:2} + C_{37:3}$ and the total mass accumulation rate at IODP Site U1419 for the past 54 ka. (a) Coccoliths (average per field of view—FoV), (b) total diatom concentration (valves g^{-2}, red line), (c) $U^{K'}_{37}$-based sea-surface temperature (SST, °C, blue line; calibrated using Müller et al., 1998), (d) $C_{37:2} + C_{37:3}$ (µg g^{-1}), and (e) total MAR (g/cm^2/ka; from Walczak et al., 2020). The total MAR is evaluated over constant timestep bins of 500 years to avoid interpretive artifacts associated with varying sample resolution. Light blue bars denote Siku Events (SE) 1–4 where IRD MAR exceeds 12 g cm^2 ka (Walczak et al., 2020). MIS: Marine Isotope Stages.

4.3.2. Composition and Temporal Variation of Diatom Groups

Despite the sporadic occurrence of diatoms in Site U1419 sediments, the preserved diatom assemblage was diverse: up to 100 species occurred (Table S1 in Supporting Information S1). To better constrain the temporal occurrence of taxa, the 29 most abundant diatoms (averagely >0.75% of the entire record) were distributed in six groups. According to their ecology, groups represent the following environmental conditions/habitats: (a) sea-ice related, (b) benthic, (c) coastal cold waters, (d) high productivity water, (e) pelagic cold water and (f) pelagic, temperate water diatoms. The species-specific composition of groups in given in Table S1.

1. The most abundant sea-ice related diatoms at Site U1419 were spores and vegetative cells of *Thalassiosira antarctica*, *Bacterosira* spp., *Fragilariopsis cylindrus* and *Porosira glacialis* (Barron et al., 2009; Hasle & Syvertsen, 1996; Müller et al., 2018; Ren et al., 2014; Sancetta, 1981)
2. *Paralia sulcata* dominated the benthic group. *Paralia sulcata* is a common component of the benthic and tycoplanktic communities, thriving in shelf and uppermost slope waters along temperate to cool seas (Round

et al., 1990). Secondary contributors to the benthic group were *Actinoptychus senarius*, *Actinoptychus vulgaris*, several species of *Cocconeis* and *Gomphonema*, *Delphineis kippae*, *Grammatophora marina*

3. Diatoms typically thriving in cold coastal waters, are today associated with low SST in oligo-to-mesotrophic waters with moderate to high dissolved silica levels, and became more abundant during intervals of weak turbulence (Crosta et al., 2012; Hasle & Syvertsen, 1996; Romero & Armand, 2010; Sancetta, 1981). Main components of this group were well-silicified *Shionodiscus trifulta*, *Shionodiscus oestrupii* var. *venrickae, Coscinodiscus oculus-iridis*, *Coscinodiscus argus*, *Cyclotella litoralis*, *Actinocyclus octonarius*, and *Thalassiosira gravida*
4. Several species of *Chaetoceros* resting spores (RS) and *Thalassionema nitzschioides* var. *nitzschioides* composed the high-productive coastal water group. Today, vegetative cells of numerous *Chaetoceros* species rapidly respond to the decay of upwelling intensity and nutrient depletion by forming endogenous resting spores (Hasle & Syvertsen, 1996). Spores of *Chaetoceros* and *T. nitzschioides* var. *nitzschioides* are common components of the upwelling assemblage in low- and high-latitude coastal areas (Nave et al., 2001; Ren et al., 2014; Romero & Armand, 2010; Romero et al., 2021)
5. Diatoms occurring in pelagic cold waters, which today mainly respond to low-to-moderate dissolved silica content in hemi-to-pelagial waters of moderate to low SST (Barron et al., 2009; Hasle & Syvertsen, 1996; Ren et al., 2014; Sancetta, 1981). *Neodenticula seminae* and *Thalassiosira nordenskioldii* contributed the most to this group at Site U1419
6. The assemblage typical of pelagic temperate waters was composed of taxa, which today thrive in open-ocean temperate waters, with low to moderate levels of dissolved silica levels and weak mixing (Crosta et al., 2012; Nave et al., 2001; Ren et al., 2014; Romero et al., 2005, 2021). At Site U1419, this group was dominated by *Roperia tesselata* and *Stephanopyxis* spp

The average of each group contributed as follows: (a) sea-ice related = 10.93 ± 9.88%, (b) benthic = 8.99 ± 12.99%, (c) cold coastal waters = 14.26 ± 13.78%, (d) high coastal productive waters = 39.51 ± 21.88%, (e) pelagic cold waters = 11.06 ± 13.82%, and (f) pelagic temperate waters = 3.10 ± 5.12% (sum of the averages = 87.85%). Due to the low occurrence of valves in several samples, we present data of the relative contribution (%) of each group only for a minor number of counted samples. The six diatom groups showed a clear temporal pattern (Figure 4). Diatoms typical of highly productive coastal waters were the main contributors to the highest maxima of diatom concentration/MAR, mainly between 54 and 29 ka (early–late MIS 3) (Figure 4). A shift in the composition of the community occurred after 29 ka onto younger times (roughly the MIS 3/2 boundary). Coastal cold water and sea-ice related diatoms were dominant between 29 and 17 ka (beginning of the deglaciation). The last deglacial showed a diverse diatom assemblage, without a particular group being dominant. Diatoms typical of pelagic cold waters dominated during the Holocene (10–2 ka).

4.4. SST

$U^{K'}_{37}$-based SSTs ranged from ~3°C to 13°C (Figure 3c). Since modern surface sediments in the GoA suggest a summer bias to the $U^{K'}_{37}$proxy (Méheust et al., 2013; Prahl et al., 2010; Tierney & Tingley, 2018), we interpreted these data to reflect summer SSTs. We expect that, as today (Stabeno et al., 2004), there is a balance between increased inputs of glacial meltwater that are likely to reduce summer SSTs, and summer surface ocean warming which may be further enhanced by stratification. We reduce the influence of the potential meltwater/sea-ice signal by calculating SSTs using $U^{K'}_{37}$, which excludes the $C_{37:4}$ alkenone. Our resulting SSTs thus reconstruct SSTs as reflecting the temperatures in which the coccolithophores were growing, which may have been influenced by several processes (discussed in Section 5.1).

Overall, SSTs remained low (~6°C) over the glacial period (MIS3 and MIS2). There is no uniform SST signal for the SE: SE4 is accompanied by a cooling then warming, SE3 is at a SST peak, and both SE2 and SE1 start with a SST peak, rapid cooling, and then warming. There were also minor millennial scale variations in SST which do not align with SE throughout the glacial stage, so that SE are not easily distinguished from the SST record. A more significant warming occurred during the deglaciation from 16 to 11.3 ka. SSTs increased more rapidly after 16 ka and remained above 8.5°C for most of the Holocene. Holocene SSTs oscillated between 8 and 13°C, in contrast to the SSTs of ~3–9°C prior to 15 ka.

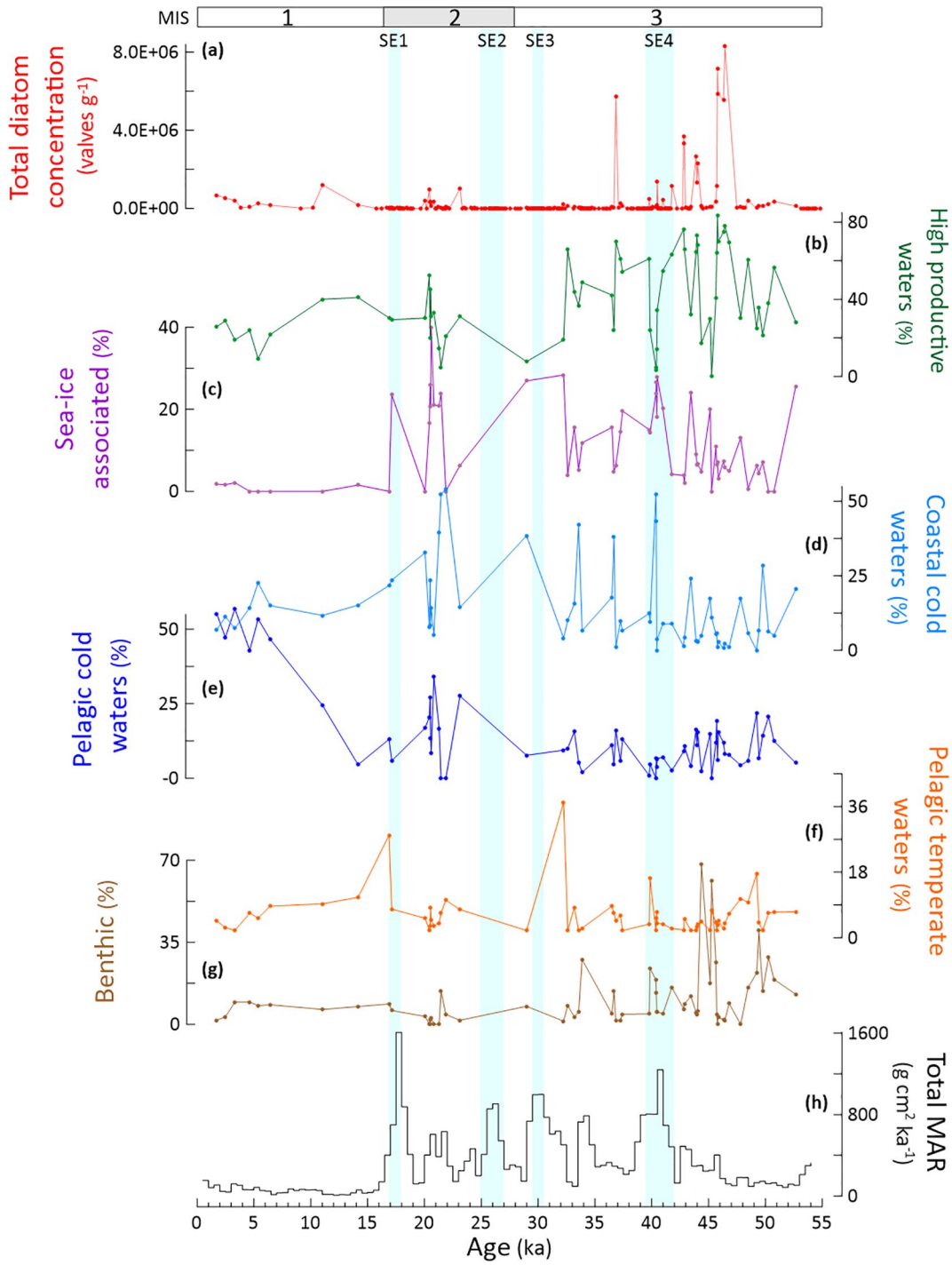

Figure 4. The diatom signal—Concentration of diatoms and the composition of the diatom assemblage at IODP Site U1419 for the past 54 ka. (a) Total diatom concentration (valves g^{-2}, red line), (c–g) cumulative percentage of diatom groups (%, lines—high-productive waters, green; sea-ice associated, crimson; coastal cold waters, light blue; pelagic cold waters, dark blue; pelagic temperate waters, orange, and benthic, red brown; for the composition of the diatom groups, see Section 4.3.2, and Supporting Information S1); and (h) total MAR (g cm^2 ka^{-1}; from Walczak et al., 2020). The total MAR is evaluated over constant timestep bins of 500 years to avoid interpretive artifacts associated with varying sample resolution. Light blue bars denote Siku Events (SE) 1–4 where IRD MAR exceeds 12 g cm^2 ka (Walczak et al., 2020). MIS: Marine Isotope Stages.

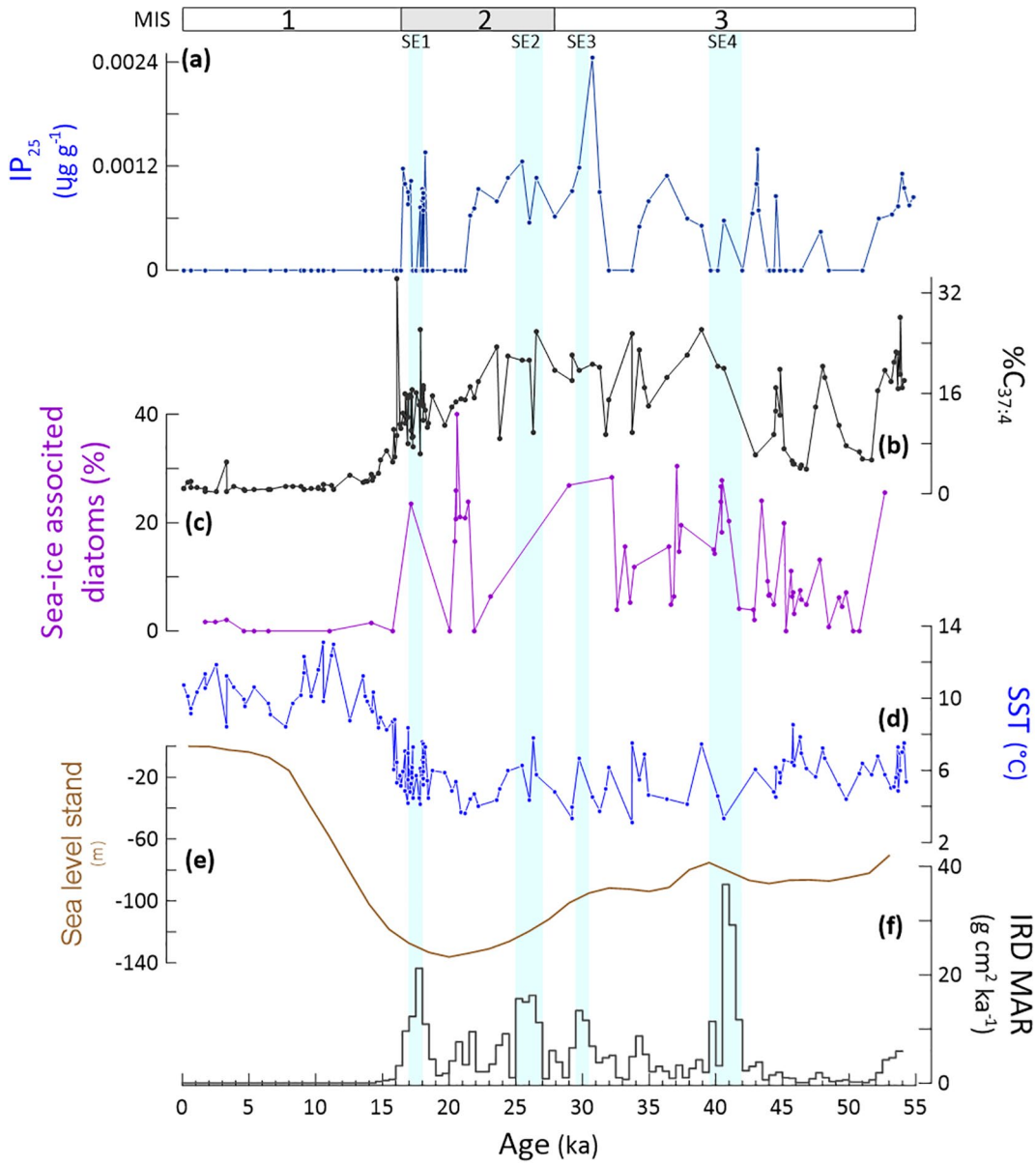

Figure 5. The sea-ice signal—Concentration of biomarkers and sea-ice associated diatoms, sea-surface temperature (SST) and mass accumulation rate of ice-rafted debris (IRD MAR) at IODP Site U1419 for the past 54 ka. (a) IP_{25} (μ g g^{-2}), (b) $\%C_{37:4}$ alkenone, (c) sea-ice associated diatoms (relative contribution—%- of the total diatom assemblage, %), (d) $U^{K'}_{37}$-based sea-surface temperature (SST, °C), (e) sea level (Waelbroeck et al., 2002) and (f) IRD MAR (g cm^2 ka^{-1}; from Walczak et al., 2020). The IRD MAR is evaluated over constant timestep bins of 500 years to avoid interpretive artifacts associated with varying sample resolution. Light blue bars denote Siku Events (SE) 1–4 where IRD MAR exceeds 12 g cm^2 ka (Walczak et al., 2020). MIS: Marine Isotope Stages.

4.5. Sea-Ice Markers

Concentrations of the spring sea-ice biomarker IP_{25} exhibited significant fluctuations over the studied sediment interval with IP_{25} mainly absent between 51.5–48.5 ka and 47–45 ka as well as during some short intervals at ca. 44.5 ka, c. 40 ka, 34.3–32 ka, 21–18.5 ka and throughout MIS1 (Figure 5a). Elevated concentrations (0.6–2.4 ng/g) were observed during and shortly before SE4 and SE3, at about 26 ka (SE2), and at about 18.7 and 17 ka (shortly before and after SE1). $C_{37:4}$ concentration maxima occurred before 16 ka and decline afterward, although there were also intervals of exceptionally low $C_{37:4}$ concentrations throughout the record (Figure 5b). While we

note similarities between the general IP_{25} pattern and $C_{37:4}$ abundances, a distinct relation between IP_{25} and $C_{37:4}$ concentrations and SE events, was not discernable.

5. Discussion

The long-term temporal evolution of reconstructed productivity, sea surface conditions (SST, sea-ice cover) and iceberg discharge at Site U1419 for the last 54 ka followed a glacial-interglacial pattern of variability. High concentrations of $CaCO_3$, coccolithophorids, bSi, and diatoms mostly occurred in MIS 3 (54–28 ka) and MIS 2 (28–17 ka). TOC values remained below 0.8% and $C_{37:2} + C_{37:3}$ alkenones below 1 μg g^{-1} until ca. 14.5 ka, then abruptly increased at 14 ka (Figures 2c and 3d). SSTs were low from MIS 3 until ca. 15.5 ka, and increased into the late deglaciation and the early Holocene (Figures 3d and 5c). Although sea-ice biomarkers (IP_{25} and $C_{37:4}$) and the sea-ice associated diatoms showed variable signals, they were predominantly present during MIS 3 and MIS 2 and decreased from 16.8 ka onward in line with increasing SSTs (Figures 4c and 5a, 5c and 5d). Superimposed on these orbital-paced variations, some proxies at Site U1419 showed suborbital-scale variations of diverse amplitude.

5.1. Productivity and Sea-Surface Conditions in the Northern Goa From MIS 3 Through MIS 2 (54–17 Ka): Impact of Icebergs and Meltwater Discharge

Located in an HNLC region of the northeastern coastal Pacific Ocean (Childers et al., 2005), Site U1419 underlies surface waters known to be largely iron-limited (Boyd et al., 2007; Martin, 1990). We argue that iron limitation largely defined the pattern of phytoplankton occurrence and the productivity in surface waters of the northern GoA during the past 54 ka.

The present-day iron limitation in the GoA largely affects the composition and dynamics of the phytoplankton communities (Childers et al., 2005; Strom et al., 2006, 2016). *In situ* iron enrichments of surface ocean waters of the GoA result in diatom blooms, demonstrating that phytoplankton growth in HNLC waters is controlled by the iron supply (Boyd et al., 2004, 2007). Since the magnitude of iron input to high-latitude oceans has changed over geological timescales (Martínez-García et al., 2011; Müller et al., 2018), it is essential to reassess its possible impact on past dynamics of primary producers. Possible mechanisms responsible for iron delivery to GoA surface waters between 54 and 17 ka might have been: (a) meltwater discharge from the northern CIS (Addison et al., 2012; Cowan et al., 2020), (b) seasonal mixing of the uppermost water column (Crusius et al., 2011), (c) aeolian input, and (d) eddy-mediated offshore transport of coastal waters (Crusius et al., 2017). Although these mechanisms might have impacted primary productivity in different ways throughout the studied interval, we assign a major role of surface water fertilization to iron delivery via iceberg and meltwater discharges from tidewater termini (Cowan et al., 2020; Crusius et al., 2017). Site U1419 was drilled on the Alaskan continental shelf, approximately 75 km west of the Bering Trough mouth (Jaeger, Gulick, & LeVay, 2014). This shelf-crossing trough was occupied by the Bering ice stream at the Last Glacial Maximum (Cowan et al., 2020, Figure 1). Because of the study site's proximity to the Bering icestream, we propose that the occurrence of the highest bulk biogenic and microfossil concentrations between early MIS 3 (c. 51.5 ka) and late MIS 2 (17 ka, shortly before the start of the last deglaciation) were due to tidewater glacier-mediated discharges of sediment-laden (iron bearing) meltwater and icebergs from the northern CIS (Penkrot et al., 2018). The seasonal mixing of the uppermost water column (Crusius et al., 2011), eddy-mediated offshore transport of coastal waters (Crusius et al., 2017), and aeolian input might have played only a subordinate role in fertilizing surficial water through iron input during MIS 3 and 2. However, the impact of aeolian input in transporting iron into GoA waters might have become more important after the deglaciation (see discussion below in Section 5.2.).

Although abundance values were generally low, coccolithophorids were more commonly present than diatoms throughout the Site U1419 record (Figures 3a and 3b). Diatom and—to a lesser extent—coccolithophorid occurrence at Site U1419 was mostly confined to short-lived events between mid MIS 3 and early MIS 1 (45–15.5 ka). Differences noted in the temporal pattern of bSi and $CaCO_3$ concentration (Figures 2a and 2b) are also seen in the record of diatoms and coccolithophorids. Differences in the timing of siliceous and calcareous occurrence in the northern GoA for the past 54 ka are thus more likely to reflect the differential response of diatoms and coccolithophorids to (a) available nutrient pools, (b) the main season of production for each phytoplankton group and/or (c) the response to dissolution throughout the water column and at the water-sediment interface. Presently,

diatoms dominate the spring phytoplankton bloom in the GoA, while coccolithophores dominates the late summer-fall phytoplankton bloom (Childers et al., 2005; Stabeno et al., 2004). However, modern studies in the GoA have been unable to link diatom (Strom et al., 2006) or coccolithophore (Lipsen et al., 2007) productivity to one single factor such as irradiance or nutrient limitation, indicating a complex oceanographic and biogeochemical system (Childers et al., 2005). The alignment of coccolithophore abundance peaks and, to a lesser extent, bSi (=diatom) concentration, with SEs (Figures 3a and 3b) suggests that the phytoplankton production was linked to enhanced nutrient availability during glacial outflow events on geological time scales.

The complex hydrographic setting in surface waters overlying waters at Site U1419 might also explain the variability of diatom group occurrence at U1419. Diatom maxima were mainly contributed by taxa typical of highly productive waters, with cold water taxa as accompanying components (Figure 4). Since species dominant in highly productive waters quickly respond to the nutrient (iron) availability, they possibly benefited from sudden inputs of iron into surficial waters in spring, following the melting of the spring sea-ice cover. This pattern altered when the occurrence of spring sea ice increased. Peaks of sea-ice associated diatoms (>30%) match intervals of low total diatom concentration and the lowered contribution of highly productive water species (Figure 4b). The sudden shifts between highly productive water and sea-ice associated species during MIS3 and SE4 might also reflect reduced spring diatom bloom due to the prolonged sea-ice season.

In addition to productivity, the concentration of bulk sediment components, fossil records, and biomarkers could be influenced by preservation or source. Carbonate dissolution can occur in waters that are oversaturated with respect to calcium carbonate because of the respiration of organic carbon in the water column and at the water/sediment interphase (Wollast & Chou, 1998). Organic carbon preservation is enhanced with high sediment burial rates or low oxygen water conditions (Canfield, 1994). Despite the increase in carbonate and TOC MAR during the SEs, the concentrations did not vary greatly over the study interval (Figures 2b and 2c), suggesting that there was a steady flux of carbon being preserved in the sediments of the northern Alaskan slope independent of glacial outflow events. The MAR maxima during the SEs could also be influenced by an increase in terrestrially derived material. Terrestrial aquatic ratio (TAR) values, however, indicate that the organic matter preserved during these intervals was of marine origin (Figure S1). Accumulation of terrestrial carbonate cannot be ruled out. Since the preservation of diatom valves at Site U1419 reflects the variable flow conditions that occurred during the entrainment and deposition of sediment from Alaska and diatoms produced in surface waters, diatom preservation is variable within different intervals and might have altered the diatom signal. However, the fact that benthic diatoms (usually more silicified than diatoms thriving in the hemipelagic and pelagic waters, Round et al., 1990) and weakly silicified taxa (such as *Fragilariopsis cylindrus*) were only accompanying components (Figure 4g), this suggests that the preserved diatom assemblage is representative of the main diatom community which occurred in waters overlying Site U1419. Exceptionally high relative values of benthic component abundance matching the lowest values of diatom concentration at 45.5–44.5, 40, 34 and 32 ka (Figure 4) supports our interpretation of benthic diatoms contributing only in a subordinate way to the U1419 diatom community.

A prominent feature of the primary producers' record is their asynchronous pattern of occurrence. Although different rates of preservation could be a factor for biogenic components, we observe certain similarities between concentrations of both inorganic and organic components for our phytoplankton groups (e.g., coccolith counts and $C_{37:2}$ + $C_{37:3}$ alkenones; Figures 3a and 3d), which are unlikely to have been driven by the same preservation factors (e.g., water column or sediment oxygenation for organic matter, dissolution processes for inorganic constituents). For example, the large peak in bSi (=diatoms) and to a lesser extent in TOC at ~46–44 ka (Figures 2a and 2c, 3a) occurred alongside a low-oxygen event identified at Site U1419 (Sharon et al., 2021; Zindorf et al., 2020), but these conditions should not have impacted the preservation of siliceous organisms (Nelson et al., 1995). Rather, a high flux of biogenic components (especially TOC, Figure 2c) to the seafloor at this time is more likely to have driven the generation of low-oxygen conditions as organic matter was respired.

Since the mean value of SST remained below 8°C between 54 and 17 ka, and no significant shifts between cooling and warming occurred during intervals of high coccolithophorid and/or diatom production (Figures 3a–3c), we argue that the occurrence of siliceous and calcareous primary producers was not influenced by low SST conditions during MIS 3 and MIS two in the northern GoA. Although the match between the sporadic occurrence of diatoms and SST variations was not consistent over the interval 54–17 ka, the long-term SST dynamics appear to have determined the changes in composition of the diatom community. The dominance of diatoms typical of cold and highly productive coastal waters between 54 and 17 ka (Figures 4b and 4d) matched the generally low

SSTs (indicative of stronger mixing, Figure 3c) and spring sea-ice occurrences indicated by IP_{25} (Figure 5a). However, spring sea-ice cover seems to have exerted no major control on coccolithophore productivity either but potentially limited diatom growth (except for SE4) as the total diatom concentration was low overall after 36 ka (i.e., since IP_{25} and $C_{37:4}$ abundances point to the recurring presence of spring sea-ice cover at Site U1419, Figures 5a and 5b).

CIS outlet glaciers along the Alaskan coast terminated with a grounded tidewater terminus, thus they slowly advanced over the course of centuries, until thinning initiated a rapid retreat that was completed within decades, stabilizing when the glacier reached shallow water depths (Cowan et al., 2020, and references therein). Once tidewater glacier retreat was initiated, the glacier's behavior was only weakly influenced by climate (e.g., SST, Pfeffer, 2007), and trough geometry and sea level primarily controlled terminus behavior (Enderlin et al., 2013). The pattern of SST variability at Site U1419 provide further evidence of the CIS controlling the coastal regime dynamics. SST variability was mostly in phase with iceberg discharges as colder SSTs were linked to SE4, 2 and 1. However, low SSTs were also recorded between SEs (e.g., between 37.5 and 34.5 ka, at 33.3 ka, 31 Ka and at c. 21 ka, Figure 3c).

5.2. SST Warming, Decrease of Bioavailable Iron and Weakened Productivity Between the Last Deglacial and Late Holocene (17-2 ka)

The abrupt decrease of MAR at Site U1419 around 17 ka (Figure 2d) signaled the early stages of glaciers' stagnation or retreat into the last deglaciation (Cowan et al., 2020). The long-term glacial retreat and sea level rise associated with the last deglacial (Figure 5) led to a flooding of the coastal plain along northern Alaska. Remobilized iron originating from the newly inundated Alaskan shelf might have fueled primary productivity events after the LGM and in turn contributed to sedimentary anoxia (Davies et al., 2011; Sharon et al., 2021; Zindorf et al., 2020). While sea-ice indicators then return to zero and SSTs reach maximum values between 11.5 and 9 ka (Figure 5), highest TOC content and elevated $C_{37:2} + C_{37:3}$ concentrations (Figures 2c and 3d) are observed between 11 and 10 ka at Site U1419. This observation is in line with a widespread phenomenon along the Alaskan margin during the last deglaciation (Addison et al., 2012; Barron et al., 2009; Davies et al., 2011), and provides additional evidence of higher productivity due to the sudden fertilization of surface coastal waters. Regarding the low MAR during this interval, elevated TAR (Figure S1) shows that there was enhanced transport of terrestrial organic matter to U1419, but we conclude that this was not carried by meltwater, as there is no associated increase in the sedimentation rate nor elevated MAR (Figure 2).

There is a noticeable millennial-scale variability of SST superimposed on a significant warming trend between 17 and 9 ka, which is accompanied by short-term fluctuations and an overall decrease in the abundance of IP_{25} and $C_{37:4}$ until 15.5 ka (Figure 5). These rapid variations suggest that a readvance of sea-ice coverage developed, perhaps in response to meltwater discharge from retreating glaciers. In line with the SST warming during the last deglacial, an increase in the contribution of diatoms thriving in pelagic, more temperate waters occurred between 14 and 11 ka, with lessened contribution of coastal cold and highly productive waters (unfortunately only four samples with a statistically significant number of valves can be considered; Figure 4). Similar observations on the shift of diatom species composition are known for the nearby core EW0408-85CJ (Barron et al., 2009).

The overall low IRD after 16 ka (Figure 2d) followed the glacier retreat scenario coupled with SST warming (confirming the trend observed at Site U1419 in the site survey core by Praetorius et al., 2015), a highly stratified uppermost water column (=weak mixing, Royer & Grosch, 2006), and weakened iceberg-mediated iron fertilization of the ocean surface. An increasingly stratified uppermost water column during the Holocene led to (a) the decreased resuspension of sediments, as well as (b) the reduction of iron delivery into shelf waters (Crusius et al., 2017).

The Holocene as preserved at Site U1419 recorded only minor environmental changes. The only striking events occurred during the early Holocene when peaks in coccolith concentration and TOC% between 10.5 and 9.5 ka, and $C_{37:2} + C_{37:3}$ alkenone concentration at c. 11 ka are observed (Figures 2 and 3; not shown in total MAR), alongside a SST warming (Figure 3c). Surface waters overlying Site U1419 then gradually cooled to c. 8°C until 7.5 ka, followed by warming through the late Holocene (8.5–12°C, Figure 3d). The higher contribution (50%–55%) of diatoms typical of pelagic cold waters after 7 ka matches well the warming recorded by the $U^{K'}_{37}$-based

temperatures (Figure 3c) and the lowered surface water production (Barron et al., 2009). The Site U1419 record displayed no indication of significant CIS discharge after 7 ka.

With decreased extension of the CIS after the last deglaciation, other mechanisms of iron delivery might have become more important. Local sources of dust include extensive areas along the southern Alaskan coastline where the glacier melting season lasts several months (Neal et al., 2010), exposing dust in glacierized river valleys (Crusius et al., 2011) which can then be carried over hundreds of kilometers beyond the shelf break in late autumn dust storms (Crusius et al., 2011; Schroth et al., 2017). Following present-day analogs (Crusius et al., 2011, 2017), we propose that vast areas in Alaska became more active sources of dust for bioavailable iron after the last deglaciation throughout the late Holocene. However, their impact on primary producers seems to be less crucial beyond the Alaskan continental shelf, since - except for the coccolithophorid maximum between 10.5 and 9.5 ka—primary producers' values resemble those recorded before the Holocene.

6. Conclusions

Our multiproxy assessment combines for the first time the study of siliceous and calcareous microfossils, bulk biogenic components, biomarkers, and ice-rafted debris for the reconstruction of sea-surface conditions, and sea-ice occurrence at IODP Site U1419 off Alaska for the past 54 ka. This multiproxy approach allows us to investigate the forcings driving paleoenvironmental change of upper ocean properties in the high-latitude northeastern Pacific on orbital and suborbital timescales.

Retreat of the CIS and the associated meltwater discharge actively defined both the orbital and suborbital timescales of productivity and sea-surface oscillations in the northern GoA. Bioavailable iron (mainly linked to iceberg discharge) largely controlled the pattern of primary productivity occurrence in waters overlying Site U1419.

The occurrence of siliceous and calcareous primary producers at Site U1419 is not consistently linked with SST variability over the entire record. SST changes were not linked to marine producers' dynamics on the suborbital timescale during MIS 3 and MIS 2, suggesting that SST is not a primary forcing of productivity change on these timescales.

Despite minor productivity peaks, less favorable conditions for primary producers prevailed between the last deglaciation (17-11 ka) and the late Holocene. Compared to MIS3 and MIS2, the significant reduction of CIS cover after the last deglaciation and weakened meltwater discharge into the northern GoA negatively impacted productivity in surface waters overlying the Alaskan slope.

Our multiproxy reconstruction suggests that iron fertilization actively fueled primary productivity in the HNLC waters adjacent to Alaskan continental ice sheets during the Late Pleistocene. This study supports the scenario of the GoA representing an ice-proximal marine environment where primary productivity, and potentially also CO_2 draw-down, are closely linked to ice-sheet dynamics (Martin, 1990).

Acknowledgments
The authors thank the Integrated Ocean Drilling Program U.S. Implementing Organization (IODP-USIO) and the captain and crew of the D/V *JOIDES Resolution* during Expedition 341. This research used samples provided by the IODP. Funding was provided by the German Research Foundation (DFG) (RO3039/4, and MU3670/1–2), the Helmholtz Association (VH-NG-1101), the Philip Leverhulme Prize (ELM), a NERC-IODP grant (NE/L002426/1, ELM), and a U.S. Science Support Program Post-Expedition Activity award to LJL. LJL's salary is provided through NSF award OCE-1326927. LJL thanks C. Ramsey and D. Mmasa for their work collecting coccolith counts. Funding was provided by the National Science Foundation award OCE-1434945 and a post-expedition award from the U.S. Science Support Program of IODP to EAC. The thorough reviews of two anonymous reviewers and comments by the Associate Editor greatly contributed to the improvement of this paper and are greatly appreciated. Open access funding enabled and organized by Projekt DEAL.

Data Availability Statement

Data files are archived at https://doi.pangaea.de/10.1594/PANGAEA.932584.

References

Addison, J. A., Finney, B. P., Dean, W. E., Davies, M. H., Mix, A. C., Stoner, J. S., & Jaeger, J. M. (2012). Productivity and sedimentary $\delta^{15}N$ variability for the last 17,000 years along the northern Gulf of Alaska continental slope. *Paleoceanography*, *27*(1). https://doi.org/10.1029/2011pa002161

Barron, J. A., Bukry, D., Dean, W. E., Addison, J. A., & Finney, B. (2009). Paleoceanography of the Gulf of Alaska during the past 15,000 years: Results from diatoms, silicoflagellates, and geochemistry. *Marine Micropaleontology*, *72*(3), 176–195. https://doi.org/10.1016/j.marmicro.2009.04.006

Belt, S. T., Massé, G., Rowland, S. J., Poulin, M., Michel, C., & LeBlanc, B. (2007). A novel chemical fossil of palaeo sea ice: IP_{25}. *Organic Geochemistry*, *38*, 16–27. https://doi.org/10.1016/j.orggeochem.2006.09.013

Blain, S., Quéguiner, B., Armand, L., Belviso, S., Bombled, B., Bopp, L., et al. (2007). Effect of natural iron fertilization on carbon sequestration in the Southern Ocean. *Nature*, *446*(7139), 1070–1074. https://doi.org/10.1038/nature05700

Bottini, C., & Erba, E. (2018). Mid-Cretaceous paleoenvironmental changes in the western Tethys. *Climate of the Past*, *14*, 1147–1163. https://doi.org/10.5194/cp-14-1147-2018

Boyd, P. W., & Ellwood, M. J. (2010). The biogeochemical cycle of iron in the ocean. *Nature Geoscience*, *3*(10), 675–682. https://doi.org/10.1038/ngeo964

Boyd, P. W., Jickells, T., Law, C. S., Blain, S., Boyle, E. A., Buesseler, K. O., et al. (2007). Mesoscale iron enrichment experiments 1993-2005: Synthesis and future directions. *Science*, *315*(5812), 612–617. https://doi.org/10.1126/science.1131669

Boyd, P. W., Law, C. S., Wong, C. S., Nojiri, Y., Tsuda, A., Levasseur, M., et al. (2004). The decline and fate of an iron-induced subarctic phytoplankton bloom. *Nature*, *428*(6982), 549-553.

Canfield, D. E. (1994). Factors influencing organic carbon preservation in marine sediments. *Chemical Geology*, *114*(3–4), 315–329. https://doi.org/10.1016/0009-2541(94)90061-2

Childers, A. R., Whitledge, T. E., & Stockwell, D. A. (2005). Seasonal and interannual variability in the distribution of nutrients and chlorophyll a across the Gulf of Alaska shelf: 1998–2000. *Deep Sea Research II*, *52*(1), 193–216. https://doi.org/10.1016/j.dsr2.2004.09.018

Cowan, E. A., Zellers, S. D., Müller, J., Walczak, M. H., Worthington, L. L., Caissie, B. E., et al. (2020). Sediment controls dynamic behavior of a Cordilleran ice stream at the last glacial maximum. *Nature Communications*, *11*(1), 1826. https://doi.org/10.1038/s41467-020-15579-0

Coyle, K. O., Hermann, A. J., & Hopcroft, R. R. (2019). Modeled spatial-temporal distribution of productivity, chlorophyll, iron and nitrate on the northern Gulf of Alaska shelf relative to field observations. *Deep-Sea Research Part II*, *165*, 163–191. https://doi.org/10.1016/j.dsr2.2019.05.006

Crawford, W. R., Brickley, P. J., & Thomas, A. C. (2007). Mesoscale eddies dominate surface phytoplankton in northern Gulf of Alaska. *Progress in Oceanography*, *75*(2), 287–303. https://doi.org/10.1016/j.pocean.2007.08.016

Crosta, X., Romero, O. E., Ther, O., & Schneider, R. R. (2012). Climatically-controlled siliceous productivity in the eastern Gulf of Guinea during the last 40 000 yr. *Climate of the Past*, *8*(2), 415–431. https://doi.org/10.5194/cp-8-415-2012

Crusius, J., Schroth, A. W., Gassó, S., Moy, C. M., Levy, R. C., & Gatica, M. (2011). Glacial flour dust storms in the Gulf of Alaska: Hydrologic and meteorological controls and their importance as a source of bioavailable iron. *Geophysical Research Letters*, *38*(6). https://doi.org/10.1029/2010GL046573

Crusius, J., Schroth, A. W., Resing, J. A., Cullen, J., & Campbell, R. W. (2017). Seasonal and spatial variabilities in northern Gulf of Alaska surface water iron concentrations driven by shelf sediment resuspension, glacial meltwater, a Yakutat eddy, and dust. *Global Biogeochemical Cycles*, *31*(6), 942–960. https://doi.org/10.1002/2016gb005493

Davies, M. H., Mix, A. C., Stoner, J. S., Addison, J. A., Jaeger, J., Finney, B., & Wiest, J. (2011). The deglacial transition on the southeastern Alaska Margin: Meltwater input, sea level rise, marine productivity, and sedimentary anoxia. *Paleoceanography*, *26*, PA2223. https://doi.org/10.1029/2010PA002051

Duprat, L. P. A. M., Bigg, G. R., & Wilton, D. J. (2016). Enhanced Southern Ocean marine productivity due to fertilization by giant icebergs. *Nature Geoscience*, *9*(3), 219–221. https://doi.org/10.1038/ngeo2633

Enderlin, E. M., Howat, I. M., & Vieli, A. (2013). High sensitivity of tidewater outlet glacier dynamics to shape. *The Cryosphere*, *7*, 1007–1015. https://doi.org/10.5194/tc-7-1007-2013

Freeland, H. J. (2006). What proportion of the north pacific current finds its way into the Gulf of Alaska? *Atmosphere-Ocean*, *44*, 321–330. https://doi.org/10.3137/ao.440401

Guballa, J. D. S., & Peleo-Alampay, A. M. (2020). Pleistocene calcareous nannofossil biostratigraphy and gephyrocapsid occurence in Site U1431D, IODP 349, South China Sea. *Geosciences*, *10*, 388. https://doi.org/10.3390/geosciences10100388

Hartnett, H. E., Keil, R. G., Hedges, J. I., & Devol, A. H. (1998). Influence of oxygen exposure time on organic carbon preservation in continental margin sediments. *Nature*, *391*, 572–575. https://doi.org/10.1038/35351

Hasle, G. R., & Syvertsen, E. E. (1996). Marine diatoms. In C. R. Tomas (Ed.), *Identifying marine diatoms and Dinoflagellates* (pp. 5–385). Academic Press. https://doi.org/10.1016/B978-0-12-693015-3.X5000-1

Henson, S. A. (2007). Water column stability and spring bloom dynamics in the Gulf of Alaska. *Journal of Marine Research*, *65*(6), 715–736. https://doi.org/10.1357/002224007784219002

Hopwood, M. J., Bacon, S., Arendt, K., Connelly, D. P., & Statham, P. J. (2015). Glacial meltwater from Greenland is not likely to be an important source of Fe to the North Atlantic. *Biogeochemistry*, *124*(1), 1–11. https://doi.org/10.1007/s10533-015-0091-6

Jaeger, J. M., Gulick, S. P. S., LeVay, L. J. & the expedition 341 Scientists. (2014). *Proceedings of the Integrated Ocean Drilling Program* (Vol. 341). College Station, Texas. Integrated Ocean Drilling Program. https://doi.org/10.2204/iodp.proc.341.101.2014

Jaeger, J. M., Gulick, S. P. S., LeVay, L. J., Asahi, H., Bahlburg, H., Belanger, C. L., et al. (2014). Methods. In Jaeger, J. M., Gulick, S. P. S., LeVay, L. J. (Eds.), and the Expedition 341 Scientists. *Proc. IODP*. Integrated Ocean Drilling Program. https://doi.org/10.2204/iodp.proc.341.102.2014

Kim, J.-H., Schneider, R. R., Müller, P. J., & Wefer, G. (2002). Interhemispheric comparison of deglacial sea-surface temperature patterns in Atlantic eastern boundary currents. *Earth and Planetary Science Letters*, *194*(3), 383–393. https://doi.org/10.1016/s0012-821x(01)00545-3

Kipphut, G. W. (1990). Glacial meltwater input to the Alaska coastal current: Evidence from oxygen Isotope measurements. *Journal of Geophysical Research: Oceans*, *95*(C4), 5177–5181. https://doi.org/10.1029/jc095ic04p05177

Lipsen, M. S., Crawford, D. W., Gower, J., & Harrison, P. J. (2007). Spatial and temporal variability in coccolithophore abundance and production of PIC and POC in the NE subarctic Pacific during El Niño (1998), La Niña (1999) and 2000. *Progress in Oceanography*, *75*(2), 304–325. https://doi.org/10.1016/j.pocean.2007.08.004

Martin, J. H. (1990). Glacial-interglacial CO_2 change: The iron hypothesis. *Paleoceanography*, *5*, 1–13. https://doi.org/10.1029/pa005i001p00001

Martínez-García, A., Rosell-Melé, A., Jaccard, S. L., Geibert, W., Sigman, D. M., & Haug, G. H. (2011). Southern Ocean dust–climate coupling over the past four million years. *Nature*, *476*(7360), 312–315. https://doi.org/10.1038/nature10310

McIntyre, A., & Be, A. W. H. (1967). Modern coccolithophoridae of the Atlantic Ocean – I. Placoliths and cyrtoliths. *Deep Sea Research and Oceanographic Abstracts*, *14*(5), 561–597. https://doi.org/10.1016/0011-7471(67)90065-4

Méheust, M., Fahl, K., & Stein, R. (2013). Variability in modern sea surface temperature, sea ice and terrigenous input in the sub-polar North Pacific and Bering Sea: Reconstruction from biomarker data. *Organic Geochemistry*, *57*, 54–64. https://doi.org/10.1016/j.orggeochem.2013.01.008

Müller, J., Romero, O. E., Cowan, E. A., McClymont, E. L., Forwick, M., Asahi, H., et al. (2018). Cordilleran ice-sheet growth fueled primary productivity in the Gulf of Alaska, northeast Pacific Ocean. *Geology*, *46*(4), 307–310. https://doi.org/10.1130/G39904.1

Müller, J., Werner, K., Stein, R., Fahl, K., Moros, M., & Jansen, E. (2012). Holocene cooling culminates in sea ice oscillations in Fram Strait. *Quaternary Science Reviews*, *47*, 1–14

Müller, P. J., Kirst, G., Ruhland, G., von Storch, I., & Rosell-Mellé, A. (1998). Calibration of the alkenone palaeotemperature index UK-37 based on core-tops from the eastern South Atlantic and the global ocean (60°N–60°S). *Geochimica et Cosmochimica Acta*, *62*, 1757–1772

Müller, P. J., & Schneider, R. R. (1993). An automated leaching method for the determination of opal in sediments and particulate matter. *Deep-Sea Research Part I*, *40*, 425–444

Nave, S., Freitas, P., & Abrantes, F. (2001). Coastal upwelling in the canary Island region: Spatial variability reflected by the surface sediment diatom record. *Marine Micropaleontology*, *42*(1), 1–23. https://doi.org/10.1016/s0377-8398(01)00008-1

Neal, E. G., Hood, E., & Smikrud, K. (2010). Contribution of glacier runoff to freshwater discharge into the Gulf of Alaska. *Geophysical Research Letters*, *37*(6), L06404. https://doi.org/10.1029/2010GL042385

Nelson, D. M., Tréguer, P., Brzezinski, M. A., Leynaert, A., & Quéguiner, B. (1995). Production and dissolution of biogenic silica in the ocean: Revised global estimates, comparison with regional data and relationship to biogenic sedimentation. *Global Biogeochemical Cycles*, *9*(3), 359–372. https://doi.org/10.1029/95gb01070

Penkrot, M. L., Jaeger, J. M., Cowan, E. A., St-Onge, G., & LeVay, L. (2018). Multivariate modeling of glacimarine lithostratigraphy combining scanning XRF, multisensory core properties, and CT imagery: IODP site U1419. *Geosphere*, *14*(4), 1–26. https://doi.org/10.1130/GES01635.1

Pfeffer, W. T. (2007). A simple mechanism for irreversible tidewater glacier retreat. *Journal of Geophysical Research Earth Surface*, *112*(F3), F03S2. https://doi.org/10.1029/2006JF000590

Praetorius, S. K., Mix, A. C., Walczak, M. H., Wolhowe, M. D., Addison, J. A., & Prahl, F. G. (2015). North Pacific deglacial hypoxic events linked to abrupt ocean warming. *Nature*, *527*(7578), 362–366. https://doi.org/10.1038/nature15753

Praetorius, S. K., Rugenstein, M., Persad, G., & Caldeira, K. (2018). Global and Arctic climate sensitivity enhanced by changes in North Pacific heat flux. *Nature Communications*, *9*(1), 3124. https://doi.org/10.1038/s41467-018-05337-8

Prahl, F. G., Muelhausen, L. A., & Zahnle, D. L. (1988). Further evaluation of long-chain alkenones as indicators of paleoceanography conditions. *Geochimica et Cosmochimica Acta*, *52*, 2303–2310. https://doi.org/10.1016/0016-7037(88)90132-9

Prahl, F. G., Rontani, J.-F., Zabeti, N., Walinsky, S. E., & Sparrow, M. A. (2010). Systematic pattern in U37K′-temperature residuals for surface sediments from high latitude and other oceanographic settings. *Geochimica et Cosmochimica Acta*, *74*, 131–143. https://doi.org/10.1016/j.gca.2009.09.027

Prahl, F. G., & Wakeham, S. G. (1987). Calibration of unsaturation patterns in longchain ketone compositions for paleotemperature assessment. *Nature*, *330*, 367–369. https://doi.org/10.1038/330367a0

Ragueneau, O., Tréguer, P., Leynaert, A., Anderson, R. F., Brzezinski, M. A., DeMaster, D. J., et al. (2000). A review of the Si cycle in the modern ocean: Recent progress and missing gaps in the application of biogenic opal as a paleoproductivity proxy. *Global and Planetary Change*, *26*, 317–365. https://doi.org/10.1016/S0921-8181(00)00052-7

Reimer, P. J., Bard, E., Bayliss, A., Beck, J. W., Blackwell, P. G., Ramsey, C. B., et al. (2013). IntCal13 and Marine13 radiocarbon age calibration curves 0–50,000 Years cal BP. *Radiocarbon*, *55*, 1869–1887. https://doi.org/10.2458/azu_js_rc.55.16947

Ren, J., Gersonde, R., Esper, O., & Sancetta, C. (2014). Diatom distributions in northern North Pacific surface sediments and their relationship to modern environmental variables. *Palaeogeography, Palaeoclimatology, Palaeoecology*, *402*, 81–103. https://doi.org/10.1016/j.palaeo.2014.03.008

Romero, O. E., & Armand, L. K. (2010). Marine diatoms as indicators of modern changes in oceanographic conditions. In J. P. Smol, & E. F. Stoermer (Eds.), *The diatoms, applications for the environmental and Earth Sciences* (2nd ed., pp. 373–400). Cambridge University Press.

Romero, O. E., Armand, L. K., Crosta, X., & Pichon, J. J. (2005). The biogeography of major diatom taxa in southern ocean surface sediments: 3. Tropical/subtropical species. *Palaeogeography, Palaeoclimatology, Palaeoecology*, *223*(1), 49–65. https://doi.org/10.1016/j.palaeo.2005.03.027

Romero, O. E., Ramondenc, S., & Fischer, G. (2021). A 2-decade (1988–2009) record of diatom fluxes in the Mauritanian coastal upwelling: Impact of low-frequency forcing and a two-step shift in the species composition. *Biogeosciences*, *18*, 1873–1891. https://doi.org/10.5194/bg-18-1873-2021

Rosell-Melé, A., Jansen, E., & Weinelt, M. (2002). Appraisal of a molecular approach to infer variations in surface ocean freshwater inputs into the North Atlantic during the last glacial. *Global and Planetary Change*, *34*, 143–152. https://doi.org/10.1016/S0921-8181(02)00111-X

Round, F. E., Crawford, R. M., & Mann, D. G. (1990). *The diatoms. Biology and morphology of the Genera*. Cambridge University Press.

Royer, T. C., & Grosch, C. E. (2006). Ocean warming and freshening in the northern Gulf of Alaska. *Geophysical Research Letters*, *33*, L16605. https://doi.org/10.1029/2006GL026767

Sancetta, C. (1981). Oceanographic and ecologic significance of diatoms in surface sediments of the Bering and Okhotsk seas. *Deep-Sea Research*, *28*, 789–817. https://doi.org/10.1016/s0198-0149(81)80002-7

Sancetta, C., & Calvert, S. E. (1988). The annual cycle of sedimentation in Saanich inlet, British Columbia: Implications for the interpretation of diatom fossil assemblages. *Deep-Sea Research*, *35*(1), 71–90. https://doi.org/10.1016/0198-0149(88)90058-1

Sánchez-Montes, M. L., McClymont, E. L., Lloyd, J. M., Müller, J., Cowan, E. A., & Zorzi, C. (2020). Late Pliocene Cordilleran Ice Sheet development with warm northeast Pacific sea surface temperatures. *Climate of the Past*, *16*(1), 299–313. https://doi.org/10.5194/cp-16-299-2020

Schrader, H.-J., & Gersonde, R. (1978). Diatoms and silicoflagellates. In W. J. Zachariasse, W. R. Riedel, A. Sanfilippo, R. R. Schmidt, M. J. Brolsma, H. Schrader, et al. (Eds.), *Micropaleontological counting methods and techniques - an exercise on an eight meter section of the Lower Pliocene of Capo Rosello, Sicily* (pp. 129–176). Utrecht Micropaleontological Bulletin.

Schroth, A. W., Crusius, J., Gassó, S., Moy, C. M., Buck, N. J., Resing, J. A., & Campbell, R. W. (2017). Atmospheric deposition of glacial iron in the Gulf of Alaska impacted by the position of the Aleutian Low. *Geophysical Research Letters*, *44*(10), 5053–5061. https://doi.org/10.1002/2017GL073565

Schroth, A. W., Crusius, J., Sholkovitz, E. R., & Bostick, B. C. (2009). Iron solubility driven by speciation in dust sources to the ocean. *Nature Geoscience*, *2*(5), 337–340. https://doi.org/10.1038/ngeo501

Seguinot, J., Rogozhina, I., Stroeven, A. P., Margold, M., & Kleman, J. (2016). Numerical simulations of the Cordilleran ice sheet through the last glacial cycle. The *Cryosphere*, *10*, 639–664. https://doi.org/10.5194/tc-10-639-2016

Sharon, Belanger, C., Du, J., & Mix, A. (2021). Reconstructing paleo-oxygenation for the last 54,000 years in the Gulf of Alaska using cross-validated benthic foraminiferal and geochemical records. *Palaeoceanography and Paleoclimatology*, *36*, e2020PA003986. https://doi.org/10.1029/2020PA003986

Stabeno, P. J., Bond, N. A., Hermann, A. J., Kachel, N. B., Mordy, C. W., & Overland, J. E. (2004). Meteorology and oceanography of the northern Gulf of Alaska. *Continental Shelf Research*, *24*(7), 859–897. https://doi.org/10.1016/j.csr.2004.02.007

Strom, S. L., Fredrickson, K. A., & Bright, K. J. (2016). Spring phytoplankton in the eastern coastal Gulf of Alaska: Photosynthesis and production during high and low bloom years. *Deep Sea Research Part II: Topical Studies in Oceanography*, *132*, 107–121. https://doi.org/10.1016/j.dsr2.2015.05.003

Strom, S. L., Olson, M. B., Macri, E. I., & Calvin, W. M. (2006). Cross-shelf gradients in phytoplankton community structure, nutrient utilization, and growth rate in the coastal Gulf of Alaska. *Marine Ecology Progress Series*, *328*, 75–92. https://doi.org/10.3354/meps328075

Tierney, J. E., & Tingley, M. P. (2018). Bayspline: A new calibration for the alkenone Paleothermometer. *Paleoceanography and Paleoclimatology*, *33*(3), 281–301. https://doi.org/10.1002/2017PA003201

Waelbroeck, C., Labeyrie, L., Michel, E., Duplessy, J. C., McManus, J. F., Lambeck, K., et al. (2002). Sea-level and deep water temperature changes derived from benthic foraminifera isotopic records. *Quaternary Science Reviews*, *21*(1), 295–305. https://doi.org/10.1016/s0277-3791(01)00101-9

Walczak, M. H., Mix, A. C., Cowan, E. A., Fallon, S., Fifield, L. K., Alder, J. R., et al. (2020). Phasing of millennial-scale climate variability in the pacific and Atlantic oceans. *Science*, *370*(6517), 716–720. https://doi.org/10.1126/science.aba7096

Wang, J., Jin, M., Musgrave, D. L., & Ikeda, M. (2004). A hydrological digital elevation model for freshwater discharge into the Gulf of Alaska. *Journal of Geophysical Research: Oceans*, *109*(C7). https://doi.org/10.1029/2002JC001430

Wang, K. J., Huang, Y., Majaneva, M., Belt, S. T., Liao, S., Novak, J., et al. (2021). Group 2i Isochrysidales produce characteristic alkenones reflecting sea ice distribution. *Nature Communications*, *12*(1), 15. https://doi.org/10.1038/s41467-020-20187-z

Winter, A., Jordan, R. W., & Roth, P. H. (1994). Biogeography of living coccolithophores in ocean waters. In A. Winter, & W. G. Siesser (Eds.), *Coccolithophores* (pp. 161–178). Cambridge Univ. Press.

Wollast, R., & Chou, L. (1998). Distribution and fluxes of calcium carbonate along the continental margin in the Gulf of Biscay. *Aquatic Geochemistry*, *4*, 369–393. https://doi.org/10.1023/A:1009640432692

Zindorf, M., Rush, D., Jaeger, J., Mix, A., Penkrot, M. L., Schnetger, B., et al. (2020). Reconstructing oxygen deficiency in the glacial Gulf of Alaska: Combining biomarkers and trace metals as paleo-redox proxies. *Chemical Geology*. *558*, 119864. https://doi.org/10.1016/j.chemgeo.2020.119864

Ziveri, P., Baumann, K.-H., Böckel, B., Bollman, J., & Young, J. R. (2004). Biogeography of selected Holocene coccoliths in the Atlantic Ocean. In H. Thierstein, & J. Young (Eds.), *Coccolithophores: From Molecular processes to global impact* (pp. 403–428). Springer Verlag. https://doi.org/10.1007/978-3-662-06278-4_15

Reference From the Supporting Information

Sikes, E. L., Volkman, J. K., Robertson, L. G., & Pichon, J.-J. (1997). Alkenones and alkenes in surface waters and sediments of the Southern Ocean: Implications for paleotemperature estimation in polar regions. *Geochimica et Cosmochimica Acta*, *61*(7), 1495–1505. https://doi.org/10.1016/s0016-7037(97)00017-3